American Journal of Physics and Applications
2026, Vol. 14, No. 4, pp. 50–67
https://doi.org/10.11648/j.ajpa.20261404.11

Research Article

Development of Sonic Crystal Noise Barriers with Simulations and Experimental Validations in Acoustic Chamber

King-cheong Lam[1], Chin-to Wat[1], Syed Bilal Ahmed[1], Chak-yin Tang[2], Hai-hui Ruan[3], Chi-ho Wong[1], Kia Ho-yin Tsang[1], Ricky Kai-long Mak[4], Wai-keung Anthony Loh[1,*]

[1]Division of Science, Engineering and Health Studies, School of Professional Education and Executive Development, The Hong Kong Polytechnic University, Hong Kong, China

[2]Department of Industrial and Systems Engineering, The Hong Kong Polytechnic University, Hong Kong, China

[3]Department of Mechanical Engineering, The Hong Kong Polytechnic University, Hong Kong, China

[4]Department of Analytics, Operations and Systems, Kent Business School, University of Kent, Canterbury, United Kingdom

Abstract

Sonic Crystal Noise Barriers (SCNBs) exploit Bragg scattering in periodic scatterer arrays to attenuate road traffic noise without the visual and aerodynamic penalties of solid walls. Despite growing computational interest, a persistent gap remains between idealised simulation predictions and measured laboratory performance, largely because viscothermal dissipation and diffraction losses are routinely omitted from numerical models. This study presents a systematic, two-phase hybrid methodology to address this gap: first, forty-four Finite Element Method (FEM) configurations were evaluated in COMSOL Multiphysics by varying filling fraction (ff = 0.1-0.5), cylinder diameter (d = 0.02-0.1 m), and lattice constant (α) to identify parameter-dependent trends in A-weighted transmission loss (TL_a). Second, fifteen representative prototype configurations were fabricated from acrylic and tested inside an anechoic/reverberation acoustic chamber to validate the computational model across the full 50-4000 Hz range. Simulations predicted a peak TL_a of 45.8 dB for ff = 0.3, d = 0.07 m, α = 0.113 m in a 2 × 4 array, while the highest experimentally measured TL_a was 10.1 dB for ff = 0.5, d = 0.07 m, α = 0.088 m in a 2 × 6 array. Although quantitative agreement was not achieved, the rank ordering of configurations by TL_a was consistent between simulation and experiment across all five filling fractions, confirming the predictive reliability of the computational model for comparative design screening. The observed over-prediction is attributed primarily to viscothermal energy losses, diffraction effects, and material absorption not captured in the idealised 2D lossless model, which reveals that cylinder diameter and lattice constant are the primary drivers of simulated TL_a, whereas fill fraction dominates the experimental TL_a response, with a 2-row depth identified as the optimal configuration depth for mid-range diameters. These findings provide a validated, data-driven design framework for cost-effective SCNB development and clarify the modelling corrections required to improve quantitative fidelity.

*Correspondence: Wai-keung Anthony Loh (anthony.wk.loh@cpce-polyu.edu.hk)

Received: 23 August 2026; **Accepted:** 4 September 2026; **Published:** 20 September 2026

Keywords

Sonic Crystal, Noise Barrier, Transmission Loss, Filling Fraction, Finite Element Method, Acoustic Chamber, COMSOL Multiphysics, Viscothermal Effect

1. Introduction

Transportation infrastructure underpins modern economic activity and mobility, yet the associated growth in road traffic generates pervasive environmental noise that degrades urban air quality and residents' wellbeing [1]. Road traffic noise exposure is linked to sleep disturbance, cardiovascular disease, and cognitive impairment, making its mitigation a significant public-health priority [2]. Noise barriers represent the most widely deployed passive control measure along transport corridors. Conventional barriers-typically continuous concrete or steel walls-are effective at blocking sound transmission, but impose significant secondary costs: they obstruct natural ventilation and daylighting, reduce visual permeability, increase urban heat-island effects, and are often considered visually intrusive [3, 4].

To reconcile acoustic performance with environmental and aesthetic demands, researchers have increasingly investigated Sonic Crystals (SCs) as an alternative barrier technology. SCs are periodic arrangements of rigid or elastic scatterers embedded in a host fluid medium. When the periodicity of the array is comparable to the wavelength of an impinging sound wave, destructive interference between scattered waves produces frequency-selective attenuation zones known as band gaps, governed by Bragg's law [5]:

$$f_{BG} = \frac{c}{2\alpha \ \sin\theta} \tag{1}$$

where n is the diffraction order (n = 1, 2, 3, …), c is the speed of sound in the medium (≈ 343 m/s in air at 20°C), and α is the lattice constant of the periodic array. In contrast to solid barriers, open SC arrays permit airflow, light transmission, and visual openness while still providing meaningful noise attenuation within targeted frequency bands. The metric used to quantify this attenuation-the difference in sound level between the incident and transmitted fields-is the Transmission Loss (TL).

Over the past decade, a growing body of literature has explored diverse SC configurations to enhance TL performance. Koussa et al. [6] employed the Boundary Element Method (BEM) to evaluate the combined effect of scatterer shape and material on TL for highway barriers, demonstrating that the cross-sectional geometry of cylinders modifies band-gap width. Onrubia-Fontangordo et al. [7] developed a low-cost numerical model specifically for the low-frequency regime, highlighting the importance of accurate boundary treatment for frequencies below 500 Hz. Redondo et al. [8] embedded Helmholtz resonators within SC lattices to broaden the attenuation band and increase insertion loss at specific resonant frequencies. Qin et al. [9] validated three-dimensional FEM models against field measurements for sonic crystal acoustic barriers, quantifying the influence of ground reflections and meteorological conditions on in-situ performance. Pe ŕ-Torres et al. [4] extended SC design to include diffusing elements, combining Finite Difference Time Domain (FDTD) modelling with scale-model experiments to realise devices offering simultaneous noise control and acoustic diffusion. More recently, Ram ŕez-Solana et al. [10] applied SCs with resonant cavities to mitigate train brake noise, while Kralov et al. [11] examined how increasing the number of rows in cylindrical SC barriers affects frequency-dependent attenuation, finding that multi-row configurations shift and deepen band gaps. Ibarias et al. [12] demonstrated broadband low-frequency absorption in clusters of hard cylindrical rods, providing physical insights directly relevant to cylinder-based SC barrier design.

Despite these advances, a persistent challenge remains: computational predictions of TL frequently diverge from experimental measurements by substantial margins, particularly at higher frequencies. Key physical mechanisms routinely omitted from idealised simulations include viscothermal losses at scatterer surfaces, diffraction around finite-height barriers, angle-dependent reflection, and material damping within the scatterer material itself [13, 14]. Zhang and Qu [14] showed that viscous and thermal dissipation can significantly modify sound propagation in phononic crystals, especially at the Bragg-scattering frequencies where local pressure gradients are highest. Accurate modelling of these effects is essential before SC designs validated computationally can be translated to field deployment with confidence.

To address this gap, the present study adopts a systematic two-phase hybrid methodology: (1) a broad parametric FEM simulation campaign using COMSOL Multiphysics to identify the effects of filling fraction, cylinder diameter, and number of rows on TL across 44 configurations; followed by (2) acoustic chamber experiments on 15 selected prototype configurations to validate the computational model and quantify simulation–experiment discrepancies. The specific objectives are to: (i) establish a computationally validated model capable of reliable comparative screening of SCNB configurations; (ii) characterise the individual and interactive effects of the three primary geometric parameters on TL performance; and (iii) identify and quantify the principal sources of discrepancy between simulation and experiment to guide future high-fidelity modelling efforts.

2. Materials and Methods

A two-phase methodology was employed, consisting of systematic parametric simulations followed by experimental validation using physical prototypes in an acoustic chamber.

2.1. Computational Model Design

2.1.1. Model Geometry and Boundary Conditions

Two-dimensional FEM simulations were conducted in COMSOL Multiphysics [15] using the Pressure Acoustics, Frequency Domain interface. The 2D model geometry was designed to replicate the internal layout and dimensions of the physical acoustic chamber used in the validation experiments, ensuring that the computational boundary conditions matched the experimental conditions as closely as possible (Figure 1). The model comprised five sub-domains (S1–S5). Sub-domains S1 and S5, positioned at the far left and far right boundaries of the model, were configured as Perfectly Matched Layers (PMLs) to simulate an open, non-reflecting infinite domain and prevent spurious wave reflections at the numerical boundaries [16]. Sub-domain S2 (1.65 m × 1.65 m) represented the anechoic source chamber and was modelled as a non-reflective space. Sub-domain S4 (1.35 m × 1.23 m) represented the reverberation receiver chamber and was modelled as a reflective space. The SC noise barrier configurations were positioned within sub-domain S3, a central aperture cell measuring 0.2 m × 0.6 m, with the left boundary acting as the acoustic inlet and the right boundary as the outlet. A broadband sound source operating across 50–4000 Hz was applied at the inlet boundary.

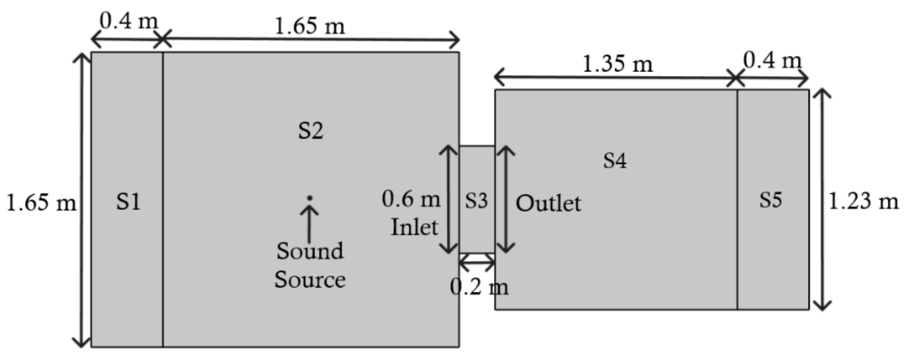

Figure 1. *Layout and dimensions of the computational model with reference to the acoustic chamber.*

2.1.2. Parametric Configurations of the Sonic Crystal Array

The acoustic performance of SC noise barriers is governed by three primary geometric parameters: the filling fraction (ff), the cylinder diameter (d), and the lattice constant (α). The filling fraction ff quantifies the proportion of the cross-sectional area of the unit cell occupied by the scatterer material. For a rectangular SC array, ff, d, and α are related by:

$$ff = \frac{\pi d^2}{4\alpha^2} \quad (2)$$

from which α is derived for each prescribed combination of ff and d (Figure 2). The number of columns was then determined as the integer number of unit cells fitting within the fixed 0.6 m aperture width of S3.

A total of 44 simulation configurations were defined by crossing five filling fractions (ff = 0.1, 0.2, 0.3, 0.4, 0.5), four cylinder diameters (d = 0.02, 0.05, 0.07, 0.1 m), and up to four row depths (1–4 rows). Configurations for which the total array height would exceed the fixed 0.6 m aperture dimension were classified as physically infeasible (N/A) and excluded from both simulation and experiment. The full parameter matrix, together with the resulting lattice constants and number of columns, is summarised in Table 1.

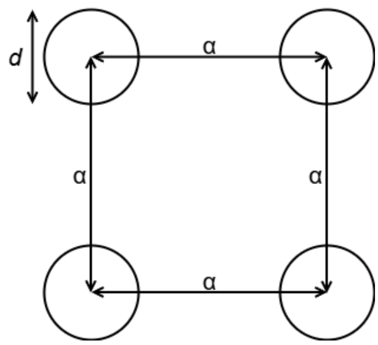

Figure 2. *Definition of lattice constant (α) and cylinder diameter (d) in a rectangular SC array.*

Table 1. *Defined SC configurations for simulations. N/A indicates configurations physically incompatible with the defined aperture dimension.*

ff	d (m)	α (m)	No. Columns	1 Row	2 Rows	3 Rows	4 Rows
0.1	0.02	0.056	10	✓	✓	✓	✓
0.1	0.05	0.140	3	✓	✓	N/A	N/A
0.1	0.07	0.196	2	✓	N/A	N/A	N/A
0.2	0.02	0.040	14	✓	✓	✓	✓
0.2	0.05	0.099	5	✓	✓	N/A	N/A
0.2	0.07	0.139	3	✓	N/A	N/A	N/A
0.2	0.10	0.198	2	✓	N/A	N/A	N/A
0.3	0.02	0.032	17	✓	✓	✓	✓
0.3	0.05	0.081	6	✓	✓	N/A	N/A
0.3	0.07	0.113	4	✓	✓	N/A	N/A
0.3	0.10	0.162	3	✓	N/A	N/A	N/A
0.4	0.02	0.028	20	✓	✓	✓	✓
0.4	0.05	0.070	7	✓	✓	✓	N/A
0.4	0.07	0.098	5	✓	✓	N/A	N/A
0.4	0.10	0.140	3	✓	N/A	N/A	N/A
0.5	0.02	0.025	23	✓	✓	✓	✓
0.5	0.05	0.063	8	✓	✓	✓	N/A
0.5	0.07	0.088	6	✓	✓	N/A	N/A
0.5	0.10	0.125	3	✓	N/A	N/A	N/A

Configurations that are physically impossible to be accommodated inside the defined dimension.

2.1.3. Evaluation Metric in Simulations

For each configuration, the simulated transmission loss (TL_{sim}) was computed from the ratio of acoustic sound intensity at the inlet (I_{in}) to the intensity at the outlet (I_{out}):

$$TL_{sim} = 10Log_{10}\left(\frac{I_{in}}{I_{out}}\right) \quad \text{[dB]} \tag{3}$$

Results were evaluated and averaged over the 1/3-octave band spectrum from 50 Hz to 4000 Hz. A-frequency weighting was subsequently applied to the 1/3-octave band levels at both the inlet and outlet prior to computing TL_a, so as to represent attenuation in terms perceptually relevant to human hearing, in accordance with IEC 61672-1: 2013 [17]. TL_a (the A-weighted transmission loss) served as the primary performance metric for comparative ranking across configurations.

2.2. Experimental Setup and Prototype Fabrication

2.2.1. Acoustic Chamber Configuration

Physical experiments were conducted in a purpose-built dual-chamber acoustic facility comprising an anechoic source room and a reverberation receiver room separated by a central aperture panel (Figure 4). The aperture opening measured 60 cm (width) × 60 cm (height), into which the SC prototypes were installed. This layout directly mirrors the S2–S3–S4 partition in the simulation model, allowing direct comparison between experimental and computational TL values. A loudspeaker, connected to a power amplifier and a laptop computer, was placed centrally within the anechoic chamber and elevated to align axially with the aperture centre, ensuring normal incidence of the acoustic wave on the noise barrier (Figure 3).

A broadband signal covering 50–4000 Hz was emitted at a time-averaged incident level of 71 dB (A). The mean background noise level in the chamber during testing was 33.1 dB (A), providing a signal-to-noise ratio exceeding 37 dB across the measurement band.

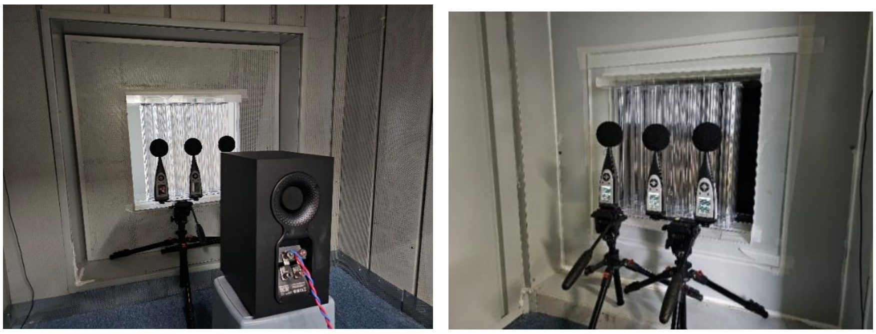

(a) (b)

***Figure 3**. Setup of physical experiment in the acoustic chamber: (a) Measuring sound level at the inlet with a speaker and 3 sound level meters in front of the noise barrier; (b) Measuring sound level at the outlet with 3 sound level meters behind the noise barrier.*

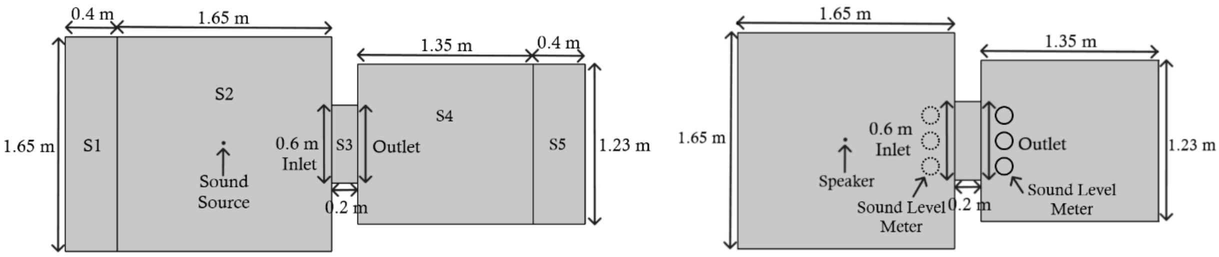

(a) (b)

***Figure 4**. Comparison between simulation model and physical acoustic chamber: (a) Layout and dimensions of simulation model; (b) Layout and dimensions of physical acoustic chamber.*

2.2.2. Prototype Construction

SC prototypes were fabricated from acrylic cylinders, each 50 cm tall. Cylinders were mounted within a rigid acrylic frame dimensioned to fit within the 60 cm × 58 cm aperture (2 cm shorter than the chamber height to allow installation), with a 2 cm gap at the top sealed with a flat acrylic plate to prevent flanking transmission (Figure 5). Two 4 cm-thick acrylic platforms at the top and bottom of the frame provided structural support for the cylinders, which were secured with adhesive putty at both contact points to eliminate rattle and maintain positional accuracy throughout repeated measurements.

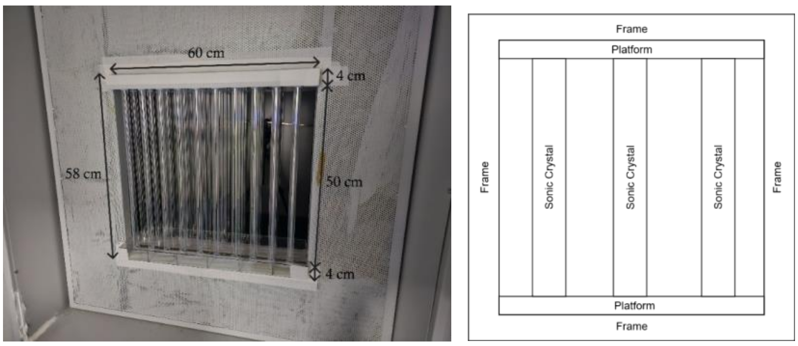

(a) (b)

***Figure 5**. Constructed and illustrated noise barrier: (a) Photograph of noise barrier installed in the acoustic chamber with key dimensions annotated; (b) Schematic illustration of the different structural components of the noise barrier.*

2.2.3. Measurement Protocol and TL Calculation

Three calibrated sound level meters (Brüel & Kjær Model 2245) were placed directly in front of the noise barrier to measure the incident sound intensity (I_{in}). The meters were then immediately relocated to the rear of the barrier for the transmitted measurement (I_{out}), with the loudspeaker emitting an identical signal. All measurements were made at the 1/3-octave band level. The experimental transmission loss (TL_{exp}), corrected for background noise, was calculated as:

$$TL_{exp} = 10log_{10}\left(\frac{I_{in}-I_{BG}}{I_{out}-I_{BG}}\right) \quad [\text{dB}] \tag{4}$$

where I_{BG} is the background noise intensity. A-weighting was applied to the measured 1/3-octave spectra at both positions before computing TL_a, consistent with the simulation evaluation protocol [17]. Each configuration was measured in triplicate with each measurement lasting 30 seconds; the reported TL_a is the mean of three repeat measurements.

2.3. Validation Strategy

The numerical validation was cross-checked using the reported work of Sharma et al. [18] in Supplementary Material section. The transmission-loss pattern against frequency was found to be consistent with previously reported of periodic acoustic barriers as shown in Figure 13. This agreement provides independent verification of the numerical formulation and implementation employed in the present work.

Experimental validation of the computational model followed a two-tier approach based on the framework described by Sargent [19]. First, the relative performance ranking of configurations was verified: configurations performing at three distinct levels (low, medium, and high TL_a) within each filling fraction were selected for physical testing, spanning the full range of ff = 0.1 to 0.5 and d = 0.02 to 0.1 m. A total of 15 configurations out of 44 were fabricated and tested. The consistency of rank ordering between simulation and experiment across all five filling fractions was used as the primary validation criterion. Second, frequency-domain waveforms of TL versus frequency were compared between simulation and experiment to diagnose frequency-specific discrepancies and inform model refinement.

3. Results and Discussion

3.1. Parametric Simulation Study

All 44 feasible configurations were simulated and the A-weighted transmission loss TL_a for each is summarised in Table 2. The overall simulated TL_a ranged from 39.7 dB (lowest performers) to 45.8 dB (best performer), a spread of 6.1 dB across the full parameter space.

Table 2. *A-weighted transmission loss (TL_a, dB) for all SC configurations in simulation. N/A denotes physically infeasible configurations. The optimal result is shown in bold.*

ff	d (m)	α (m)	Columns	1 Row TL_a (dB)	2 Rows TL_a (dB)	3 Rows TL_a (dB)	4 Rows TL_a (dB)
0.1	0.02	0.056	10	40.1	40.3	40.9	40.3
0.1	0.05	0.140	3	41.1	40.2	N/A	N/A
0.1	0.07	0.196	2	41.9	N/A	N/A	N/A
0.2	0.02	0.040	14	40.9	40.4	40.4	39.7
0.2	0.05	0.099	5	42.2	44.8	N/A	N/A
0.2	0.07	0.139	3	41.0	N/A	N/A	N/A
0.2	0.10	0.198	2	44.7	N/A	N/A	N/A
0.3	0.02	0.032	17	41.0	40.2	40.1	40.7
0.3	0.05	0.081	6	42.7	40.9	N/A	N/A
0.3	0.07	0.113	4	41.0	45.8	N/A	N/A
0.3	0.10	0.162	3	43.5	N/A	N/A	N/A
0.4	0.02	0.028	20	41.5	40.4	40.1	39.7
0.4	0.05	0.070	7	41.3	40.2	41.5	N/A
0.4	0.07	0.098	5	42.1	42.5	N/A	N/A
0.4	0.10	0.140	3	44.2	N/A	N/A	N/A

ff	d (m)	α (m)	Columns	1 Row TL_a (dB)	2 Rows TL_a (dB)	3 Rows TL_a (dB)	4 Rows TL_a (dB)
0.5	0.02	0.025	23	42.0	41.6	40.6	40.3
0.5	0.05	0.063	8	41.4	40.3	45.1	N/A
0.5	0.07	0.088	6	44.4	45.1	N/A	N/A
0.5	0.10	0.125	3	41.5	N/A	N/A	N/A

3.1.1. Effect of Cylinder Diameter on TL_a

Figure 6 presents TL_a as a function of cylinder diameter at each filling fraction for 1-row and 2-row configurations. A general trend of increasing TL_a with cylinder diameter is observed at constant ff, which is physically consistent with the Bragg scattering mechanism: larger cylinders present a greater acoustic cross-section, increasing the intensity of scattered waves and the depth of the resulting band gap. This trend holds clearly at ff = 0.1 (TL_a rising from 40.1 dB at d = 0.02 m to 41.9 dB at d = 0.07 m), ff = 0.3 (40.1–45.8 dB across the diameter range), and ff = 0.4 (39.7–44.2 dB).

However, the diameter–TL_a relationship is not monotonic in all cases. Notable exceptions include d = 0.07 m at ff = 0.2 and 0.3 for single-row configurations, and d = 0.05 m at ff = 0.4 and 0.5 for 1- and 2-row configurations. These anomalies suggest that when a given combination of d and α places a Bragg frequency outside the heavily A-weighted 1000–4000 Hz octave bands, the broadband A-weighted average TL does not necessarily increase monotonically with diameter. Maximising TL_a for a traffic noise spectrum therefore requires that the principal band gap be centred near the A-weighting peak sensitivity range, not merely that the scatterer cross-section be large.

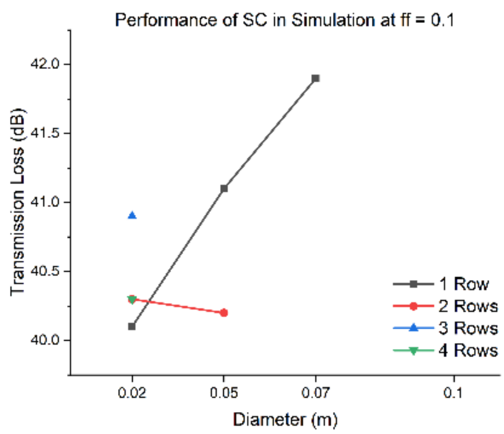

(a) ff = 0.1

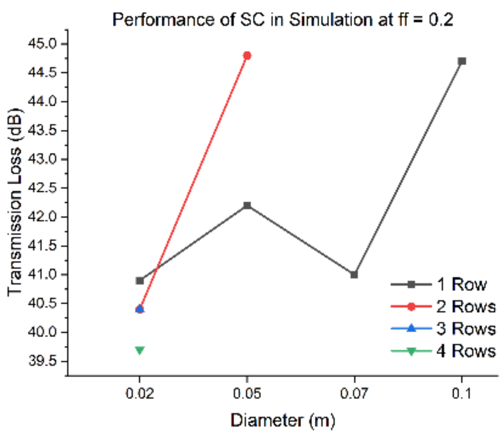

(b) ff = 0.2

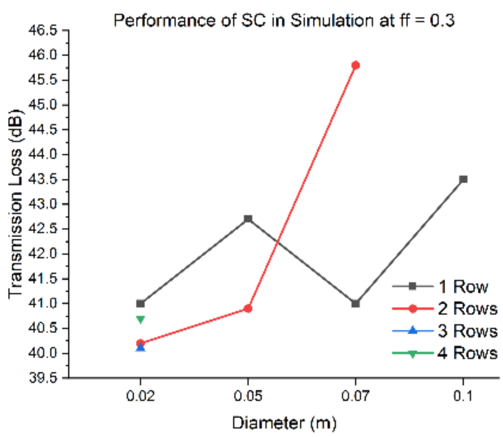

(c) ff = 0.3

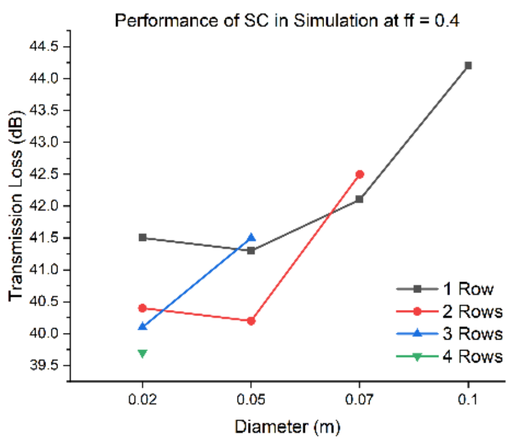

(d) ff = 0.4

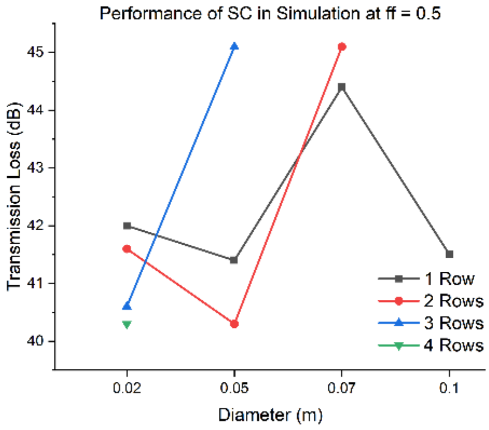

(e) ff = 0.5

Figure 6. *TL_a versus cylinder diameter of SC in simulations at different filling fractions: (a) ff = 0.1; (b) ff = 0.2; (c) ff = 0.3; (d) ff = 0.4; (e) ff = 0.5.*

3.1.2. Effect of Filling Fraction on TL_a

Figure 7 presents TL_a as a function of ff at each cylinder diameter. In contrast to the generally positive diameter effect, no consistent monotonic trend with filling fraction is observed across different diameters. At d = 0.02 m and d = 0.05 m, TL_a shows relatively modest variation across the five filling fractions (< 2 dB spread for single-row configurations at d = 0.02 m), suggesting that for small-diameter cylinders, changes in array density have limited impact on the broadband A-weighted attenuation. The most pronounced ff-dependent changes occur at larger diameters: for d = 0.07 m, TL_a peaks at ff = 0.3–0.5, and for d = 0.1 m, performance is consistently high at ff = 0.2 (44.7 dB) and ff = 0.4 (44.2 dB).

This pattern implies that filling fraction does not operate independently of diameter in determining TL performance: the effective acoustic response is governed by the combined ff–d–α triplet rather than any single parameter in isolation. Since α is jointly determined by both ff and d (Eq. 2), and it is α that controls the Bragg frequency (Eq. 1), configurations with different ff and d values but similar resulting α exhibit comparable band-gap positions and similar TL_a values. For practical design, targeting a specific road traffic noise spectrum should begin with identifying the required band-gap centre frequency (and hence α), and only then selecting the ff–d combination that delivers the desired α within the physical and cost constraints of the barrier.

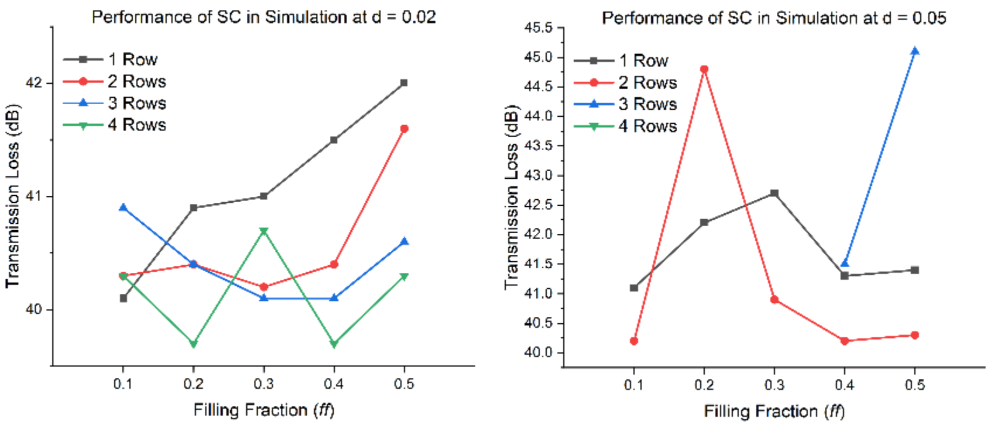

(a) d = 0.02

(b) d = 0.05 m

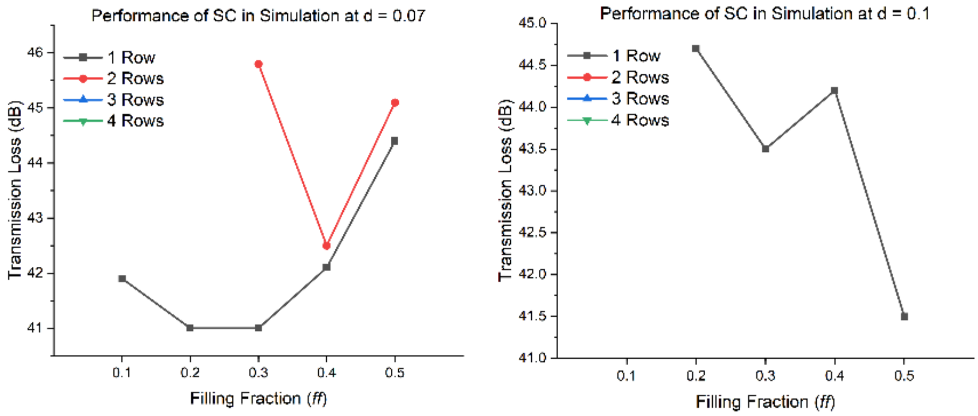

(c) d = 0.07 m (d) d = 0.10 m

Figure 7. *TL_a versus filling fraction (ff) of SC in simulations at different cylinder diameters: (a) d = 0.02 m; (b) d = 0.05 m; (c) d = 0.07 m; (d) d = 0.1 m.*

3.1.3. Effect of Number of Rows on TL_a

The influence of the number of rows is evident in Table 2, but is non-monotonic across configurations. For arrays with small-diameter cylinders (d = 0.02 m), adding rows beyond a single layer yields negligible or even slightly reduced TL_a (e.g., at ff = 0.2: 40.9 dB → 40.4 dB → 40.4 dB → 39.7 dB from 1 to 4 rows). This behaviour is consistent with findings by Kralov et al. [11], who reported that for small-cylinder SC barriers, adding rows primarily redistributes scattered energy into side lobes rather than increasing forward blockage.

In contrast, for medium-diameter configurations, an additional row can produce a substantial TL_a uplift: at ff = 0.3, d = 0.07 m, expanding from 1 to 2 rows increases TL_a from 41.0 dB to 45.8 dB-an improvement of 4.8 dB. Similarly, at ff = 0.2, d = 0.05 m, a second row raises TL_a from 42.2 dB to 44.8 dB (+2.6 dB), and at ff = 0.5, d = 0.07 m, a second row improves TL_a from 44.4 dB to 45.1 dB (+0.7 dB). This non-monotonic dependence suggests that multi-row benefits are configuration-specific and scale most favourably when the single-row configuration is already producing a substantial Bragg-band effect. For design purposes, the practical value of adding rows must be weighed against the increased material cost and reduced airflow transparency of deeper arrays.

3.1.4. Optimal Configuration from Simulation

The highest simulated TL_a of 45.8 dB was achieved by the configuration ff = 0.3, d = 0.07 m, α = 0.113 m, in a 2-row × 4-column array. This result reflects a balance between multiple competing effects: a moderate ff (0.3) delivers sufficient scattering cross-section; a medium cylinder diameter (0.07 m) and the second row of cylinders creates constructive multi-row interference that amplifies attenuation at this frequency. The 6.1 dB spread across all 44 configurations (39.7–45.8 dB) confirms that geometric parameter selection meaningfully influences SCNB performance.

3.2. Experimental Results

3.2.1. Measured TL_a Performance

Table 3 presents the measured TL_a values for the 15 prototype configurations tested in the acoustic chamber, alongside their corresponding simulation values. The average incident sound level was 71 dB (A) and the background noise level was 33.1 dB (A), providing a signal-to-noise margin of 37.9 dB. The best experimental performer, ff = 0.5, d = 0.07 m, α = 0.088 m, 2 × 6 array, achieved a TL_a of 10.1 dB. The spread across all 15 measured configurations was 2.2 dB (7.9–10.1 dB), approximately one-third of the 6.1 dB spread observed in simulations.

Table 3. *Measured TL_a (experimental) and corresponding simulated TL_a (dB) for the 15 selected SC prototype configurations.*

ff	Sim. Performance Level	Configuration	Exp. TL_a (dB)	Sim. TL_a (dB)
0.1	Low	d=0.02 m, α=0.056 m, 1×10 Array	7.9 (±0.2)	40.1
	Medium	d=0.02 m, α=0.056 m, 4×10 Array	8.3 (±0.2)	40.3
	High	d=0.07 m, α=0.196 m, 1×2 Array	8.6 (±0.3)	41.9
0.2	Low	d=0.02 m, α=0.040 m, 4×14 Array	8.7 (±0.3)	39.7

ff	Sim. Performance Level	Configuration	Exp. TL_a (dB)	Sim. TL_a (dB)
	Medium	d=0.02 m, α=0.040 m, 1×14 Array	8.8 (±0.3)	40.9
	High	d=0.05 m, α=0.099 m, 2×5 Array	9.3 (±0.4)	44.8
	Low	d=0.02 m, α=0.032 m, 3×17 Array	8.6 (±0.3)	40.1
0.3	Medium	d=0.02 m, α=0.032 m, 1×17 Array	9.1 (±0.4)	41.0
	High	d=0.07 m, α=0.113 m, 2×4 Array	9.5 (±0.5)	45.8
	Low	d=0.02 m, α=0.028 m, 4×20 Array	8.8 (±0.4)	39.7
0.4	Medium	d=0.05 m, α=0.070 m, 1×7 Array	9.1 (±0.4)	41.3
	High	d=0.10 m, α=0.140 m, 1×3 Array	9.4 (±0.5)	44.2
	Low	d=0.02 m, α=0.025 m, 4×23 Array	9.4 (±0.4)	40.3
0.5	Medium	d=0.02 m, α=0.025 m, 2×23 Array	9.9 (±0.6)	41.6
	High	d=0.07 m, α=0.088 m, 2×6 Array	10.1 (±0.5)	45.1

3.2.2. Effect of Filling Fraction on Experimental TL_a

The experimental data reveal a clear positive relationship between filling fraction and TL_a at equivalent performance levels. Across the low-performance configurations, measured TL_a increases from 7.9 dB (ff = 0.1) to 9.4 dB (ff = 0.5), a 1.5 dB gain. At the high-performance level, TL_a increases from 8.6 dB (ff = 0.1) to 10.1 dB (ff = 0.5), also a 1.5 dB gain. This positive ff–TL_a trend is consistent with the qualitative simulation prediction and with the findings of Handayani et al. [20], who reported that higher filling fractions provide greater acoustic blockage in road-traffic sound barrier models. As ff increases, the total area blocked by scatterers per unit cell grows, increasing both specular reflection at low frequencies and Bragg-band attenuation at the lattice-defined resonance frequencies.

The compressed experimental range (2.2 dB spread versus 6.1 dB in simulation) underscores that the idealised lossless simulation model substantially amplifies the apparent sensitivity of TL to parameter variations. In the physical chamber, energy dissipation mechanisms introduce a performance floor that limits the maximum achievable TL_a for this aperture size and frequency range.

3.3. Comparison of Simulation and Experimental Results

3.3.1. Consistency of Performance Rankings

The most important validation outcome concerns whether simulations correctly identify which configurations perform better than others. Examining Table 3, the rank ordering of configurations from low to high TL_a at each filling fraction is preserved between experiment and simulation in all five ff groups. Configurations designated as 'high performance' by simulation consistently achieved the highest measured TL_a values within their filling fraction group; 'low performance' simulated configurations consistently yielded the lowest measured TL_a values. This concordance is maintained across cylinders ranging from d = 0.02 m to d = 0.10 m and across filling fractions from 0.1 to 0.5, confirming that the computational model reliably predicts the comparative acoustic performance hierarchy of SCNB configurations despite its quantitative over-prediction.

3.3.2. Frequency-Domain Comparisons

Figures 8-12 present frequency-resolved TL comparisons between simulation and experiment for each filling fraction at the three performance levels. Several consistent patterns emerge across all fifteen comparisons:

Magnitude offset. Simulated TL values exceed experimental values at virtually all frequencies, with differences typically in the range of 20–40 dB at higher frequencies. This systematic offset far exceeds measurement uncertainty (estimated at < 1 dB for the calibrated B&K 2245 sound level meters) and points to the fundamental idealisation of the 2D lossless simulation model.

Low-frequency agreement. Both simulation and experiment exhibit similar gradual TL increases in the 50–400 Hz range. This agreement is expected: viscothermal boundary-layer losses scale with frequency (loss $\propto f^{1/2}$), so their relative contribution is smallest at sub-400 Hz where wavelengths greatly exceed the cylinder circumference and boundary-layer thickness [14].

High-frequency divergence and comb-filter effects. Above approximately 630 Hz, simulated TLa shows pronounced irregular fluctuations resembling a comb-filter pattern. This behaviour is characteristic of standing-wave interactions within the finite reverberation chamber [21] and reflections from rigid chamber walls, both of which modulate the received level at the microphone positions. The measured TLa remains substantially smoother, reflecting the absence of room-mode modelling within the 2D FEM domain.

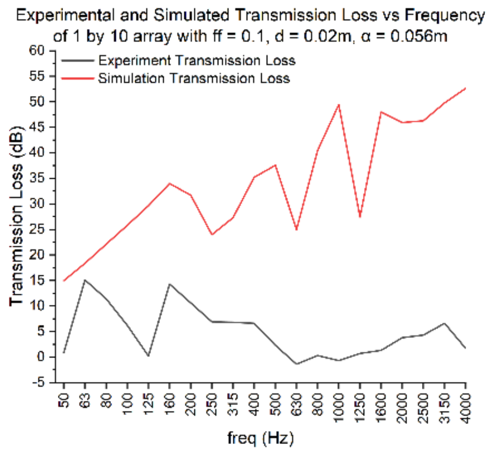

(a) 1×10 array (Low: ff=0.1, d=0.02 m, α=0.056 m)

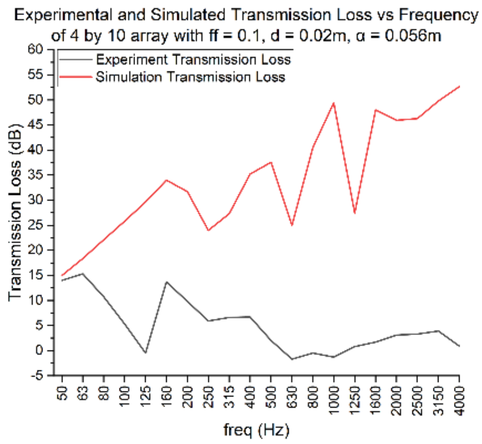

(b) 4×10 array (Medium: ff=0.1, d=0.02 m, α=0.056 m)

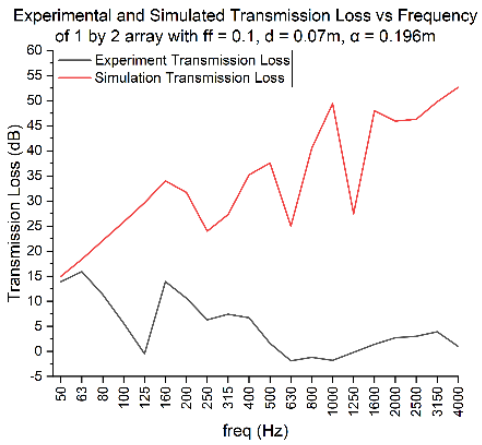

(c) 1×2 array (High: ff=0.1, d=0.07 m, α=0.196 m)

Figure 8*. Comparisons of experimental and simulated TL versus frequency for SC noise barrier at ff = 0.1 at low, medium and high performance levels. Frequency scale represents 1/3-octave band centre frequencies from 50 Hz to 4000 Hz.*

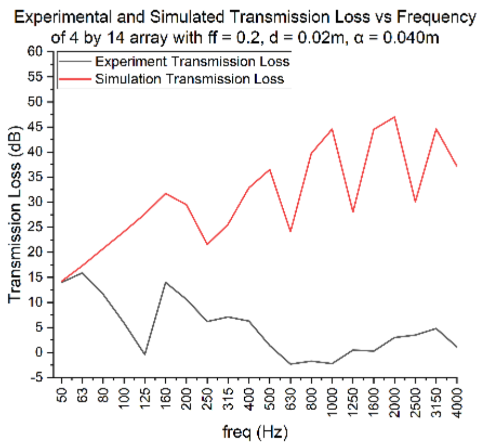

(a) 4×14 array (Low: ff=0.2, d=0.02 m, α=0.040 m)

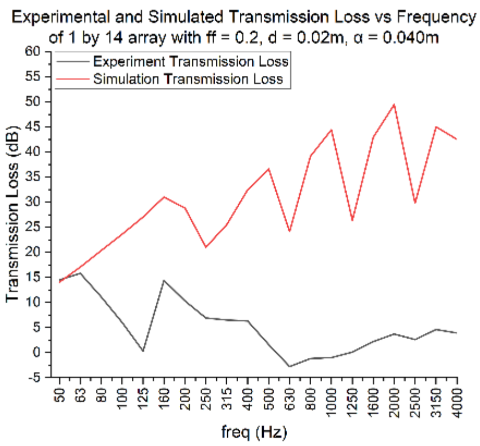

(b) 1×14 array (Medium: ff=0.2, d=0.02 m, α=0.040 m)

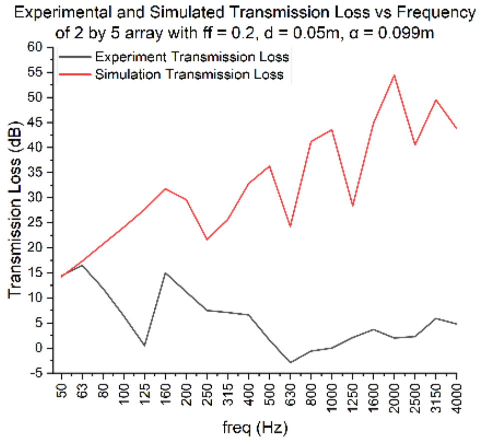

(c) 2×5 array (High: ff=0.2, d=0.05 m, α=0.099 m)

Figure 9. *Comparisons of experimental and simulated TL versus frequency for SC noise barrier at ff = 0.2 at low, medium and high performance levels. Frequency scale represents 1/3-octave band centre frequencies from 50 Hz to 4000 Hz.*

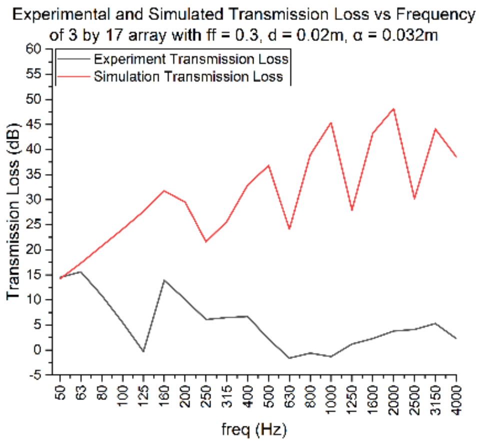

(a) 3×17 array (Low: ff=0.3, d=0.02 m, α=0.032 m)

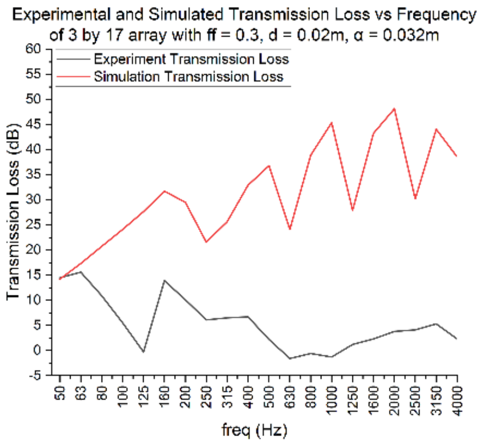

(b) 1×17 array (Medium: ff=0.3, d=0.02 m, α=0.032 m)

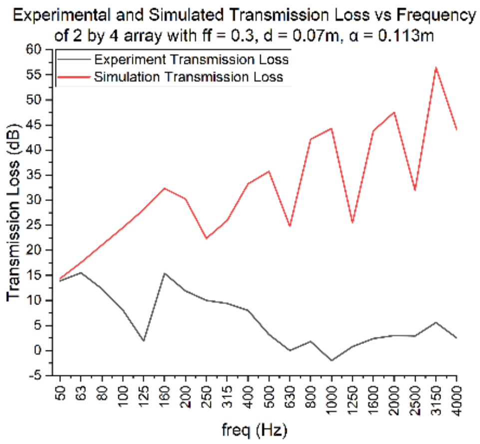

(c) 2×4 array (High: ff=0.3, d=0.07 m, α=0.113 m)

Figure 10. *Comparisons of experimental and simulated TL versus frequency for SC noise barrier at ff = 0.3 at low, medium and high performance levels. Frequency scale represents 1/3-octave band centre frequencies from 50 Hz to 4000 Hz.*

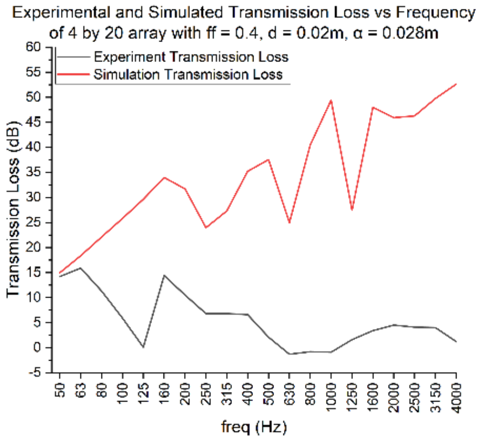

(a) 4×20 array (Low: ff=0.4, d=0.02 m, α=0.028 m)

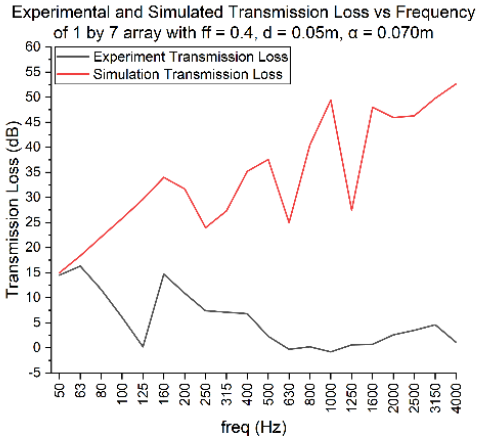

(b) 1×7 array (Medium: ff=0.4, d=0.05 m, α=0.070 m)

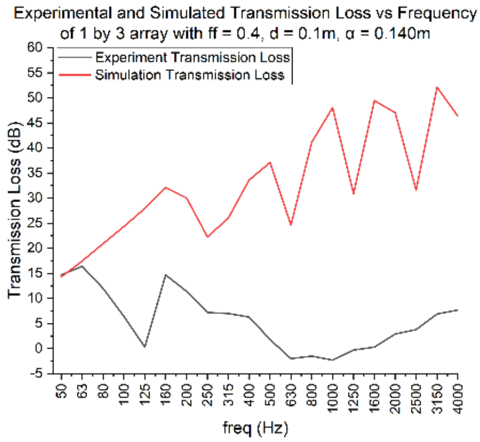

(c) 1×3 array (High: ff=0.4, d=0.10 m, α=0.140 m)

Figure 11*. Comparisons of experimental and simulated TL versus frequency for SC noise barrier at ff = 0.4 at low, medium and high performance levels. Frequency scale represents 1/3-octave band centre frequencies from 50 Hz to 4000 Hz.*

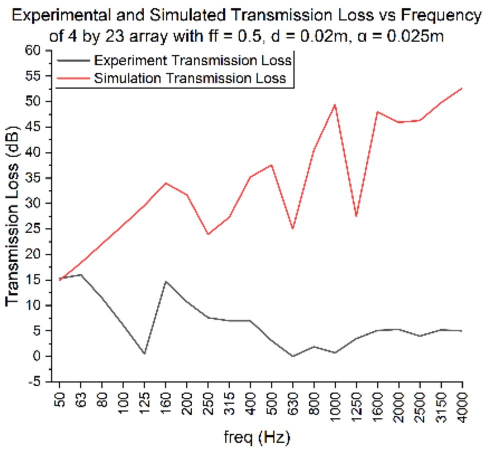

(a) 4×23 array (Low: ff=0.5, d=0.02 m, α=0.025 m)

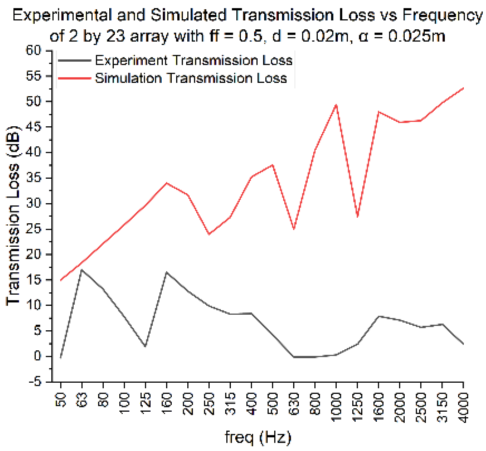

(b) 2×23 array (Medium: ff=0.5, d=0.02 m, α=0.025 m)

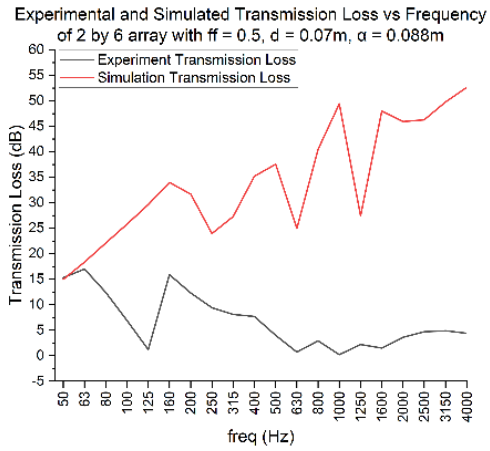

(c) 2×6 array (High: ff=0.5, d=0.07 m, α=0.088 m)

Figure 12. *Comparisons of experimental and simulated TL versus frequency for SC noise barrier at ff = 0.5 at low, medium and high performance levels. Frequency scale represents 1/3-octave band centre frequencies from 50 Hz to 4000 Hz.*

3.4. Sources of Discrepancy and Implications for Model Fidelity

3.4.1. Viscothermal Energy Losses

The main source of quantitative mismatch between simulation and experiment is the omission of viscothermal losses in the FEM model. In real SCNBs, viscous and thermal boundary layers form around each cylinder, becoming significant at kHz frequencies where Bragg scattering occurs. Prior studies [13, 14] show that these losses can reduce peak TL and substantially alter metamaterial responses. Implementing a viscothermal model in COMSOL-such as the Thermoacoustics interface-would be the most effective improvement for narrowing the simulation–experiment gap.

3.4.2. Two-Dimensional Modelling Idealisation

The 2D model cannot capture out-of-plane diffraction over the finite cylinder height (50 cm) and around the perimeter of the barrier frame. causing TL to be overestimated relative to real finite structures. Experimental studies [20] confirm that 2D algorithms deviate from 3D measurements due to angular emission and reception effects, with errors increasing at higher frequencies. Although the present study employed a two-dimensional model to enable systematic evaluation of 44 configurations within practical computational limits, future work will include selected three-dimensional simulations of representative configurations. Such models will incorporate finite cylinder height, frame geometry and over-barrier diffraction effects.

3.4.3. Implications for Practical Use of the Validated Model

The validated model offers two distinct types of utility. First, its ability to correctly rank configurations by relative TL_a performance-confirmed experimentally here-makes it a reliable and cost-effective tool for comparative design screening: multiple geometries can be evaluated computationally, and only the most promising need to be physically prototyped. This substantially reduces the experimental effort required in the barrier development cyscle [22, 23]. Second, the characterised discrepancy provides a basis for a practical correction factor specific to the present experimental geometry, material, and frequency range. These findings are consistent with published numerical–experimental comparisons for sonic crystal barriers [6, 9, 24] and reinforce the consensus that lossless 2D FEM models are best used for parametric ranking rather than absolute TL prediction.

4. Conclusion

This study developed and validated a hybrid simulation–experiment framework for Sonic Crystal Noise Barrier (SCNB) design, systematically exploring the influence of filling fraction (ff = 0.1–0.5), cylinder diameter (d = 0.02–0.1 m), and number of rows (1–4) on A-weighted transmission loss (TL_a) across 44 FEM configurations and 15 experimental prototypes. The principal conclusions are as follows:

1) Parameter effects on simulated TL_a. Increasing cylinder diameter generally increases TL_a at constant filling fraction, with the dominant mechanism being the alignment of the Bragg frequency with the A-weighted sensitive frequency range. Filling fraction shows no consistent monotonic effect when examined independently, because its influence is mediated through the lattice constant α. Adding a second row of cylinders can significantly enhance TL_a for medium-diameter configurations (+4.8 dB for the optimal case), but delivers diminishing or negligible returns for small-diameter dense arrays.

2) Optimal simulated configuration. The configuration ff = 0.3, d = 0.07 m, α = 0.113 m in a 2 × 4 array achieved the highest simulated TL_a of 45.8 dB producing the superior attenuation of this configuration.
3) Experimental performance. Measured TL_a values ranged from 7.9 to 10.1 dB across the 15 prototypes-a 2.2 dB spread-significantly lower in absolute magnitude but qualitatively consistent with simulation rankings. The highest experimental TL_a (10.1 dB) was achieved by ff = 0.5, d = 0.07 m, α = 0.088 m in a 2 × 6 array. A positive relationship between filling fraction and measured TL_a was confirmed across all five ff groups.
4) Model validation. The performance ranking of configurations from low to high TL_a was preserved between simulation and experiment for all five filling fractions, validating the computational model's predictive reliability for comparative design screening. Quantitative over-prediction is attributed primarily to viscothermal boundary-layer losses at cylinder surfaces, 2D idealisation of the finite cylinder geometry, and material absorption in the acrylic prototypes.

The validated framework established here provides an efficient, scalable, and cost-effective design tool for SCNB development, reducing the need for extensive physical prototyping during early design stages. Future simulations should incorporate viscothermal loss modelling and extend the geometry to 3D to capture over-barrier diffraction, and include realistic material damping coefficients for the chosen scatterer material. These enhancements are expected to substantially close the quantitative gap between simulation and experiment. Future experimental work should pursue field-scale validation under realistic meteorological and ground-reflection conditions, investigate hybrid SC designs incorporating local resonators or absorptive in-fills for broadband and low-frequency attenuation, and apply the validated model to optimise SCNB configurations for specific road traffic noise spectra in urban deployment scenarios.

Abbreviations

BEM	Boundary Element Method
DFT	Density Functional Theory
FDTD	Finite Difference Time Domain
FEM	Finite Element Method
IEC	International Electrotechnical Commission
PML	Perfectly Matched Layer
SC	Sonic Crystal
SCNB	Sonic Crystal Noise Barrier
TL	Transmission Loss
TL_a	A-weighted Transmission Loss
TL_{exp}	Experimental Transmission Loss
TL_{sim}	Simulated Transmission Loss
FF	Filling Fraction
d	Cylinder Diameter
α	Lattice Constant
I_{in}	Inlet Sound Intensity
I_{out}	Outlet Sound Intensity
I_{BG}	Background Noise Intensity

Acknowledgments

We gratefully acknowledge the provision of the anechoic chamber and related equipment with the kind assistance of Dr. Junot Liang.

Author Contributions

King-cheong Lam: Formal Analysis, Investigation, Methodology, Writing – review & editing

Chak-yin Tang: Software

Hai-hui Ruan: Software

Chi-ho Wong: Software

Kia Ho-yin Tsang: Data curation, Formal Analysis, Investigation, Methodology, Visualization, Writing – original draft, Writing – review & editing

Ricky Kai-long Mak: Conceptualization, Formal Analysis, Funding acquisition, Methodology, Writing – review & editing

Wai-keung Anthony Loh: Funding acquisition, Supervision

Funding

This work was fully supported by a grant from the Research Grants Council of the Hong Kong Special Administrative Region, China (RGC Project Ref. No. UGC/FDS24/E12/23).

Data Availability Statement

The data is available from the corresponding author upon reasonable request.

Conflicts of Interest

The authors declare no conflicts of interest.

Appendix

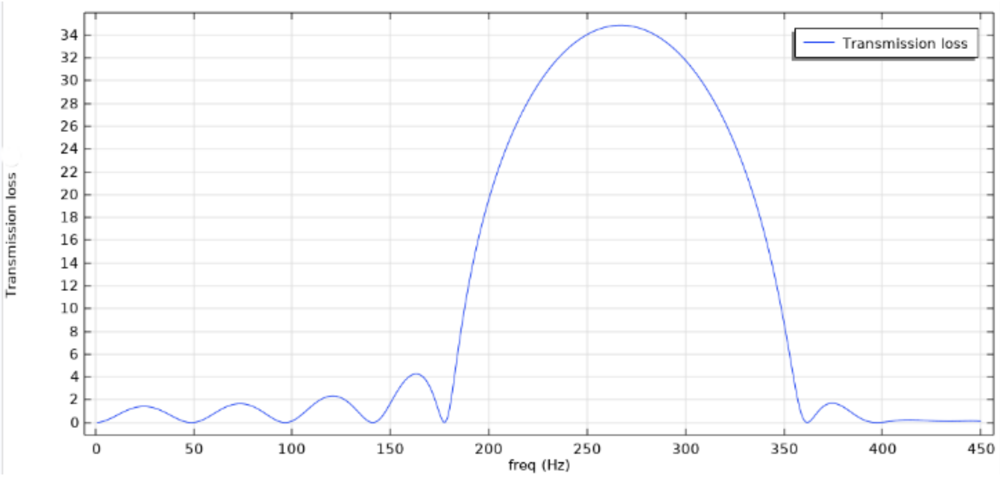

(a) The simulation result from this work using the model from Sharma et al. [18].

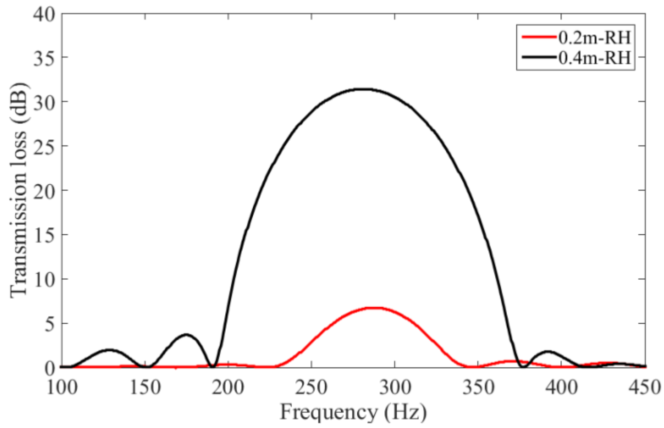

(b) The simulation result reported from Sharma et al. [18].

Figure 13. *The validation of the simulation results in this study was conducted through comparison with the model proposed by Sharma et al. [18].*

References

[1] L. Fredianelli, L. Del Pizzo, and G. Licitra, "Recent developments in sonic crystals as barriers for road traffic noise mitigation," Environments, vol. 6, no. 2, p. 14, 2019. https://doi.org/10.3390/environments6020014

[2] G. C. Tocci, Handbook of Acoustical Measurements and Noise Control, 3rd ed. New York, NY, USA: J. Acoust. Soc. Am. 1993, p.3532. https://doi.org/10.1121/1.405398

[3] Federal Highway Administration, U. S. Dept. of Transportation, "Highway traffic noise barriers at a glance." [Online]. Available: https://www.fhwa.dot.gov/environment/noise/noise_barriers/design_construction/keepdown.cfm

[4] M. P. Peiró-Torres, M. J. Parrilla Navarro, M. Ferri, J. M. Bravo, J. V. Sánchez-Pérez, and J. Redondo, "Sonic crystals acoustic screens and diffusers," Appl. Acoust., vol. 148, pp. 399–408, 2019. https://doi.org/10.1016/j.apacoust.2019.01.004

[5] P. Gulia and A. Gupta, "Multi-directional sound reduction by slitted sonic crystal," in Advances in Mechanical Engineering, Singapore: Springer Singapore, 2020, pp. 1099–1108. https://doi.org/10.1007/978-981-15-0124-1_97

[6] F. Koussa, J. Defrance, P. Jean, and P. Blanc-Benon, "Acoustical efficiency of a sonic crystal assisted noise barrier," Acta Acust. United Acust., vol. 99, no. 3, pp. 399–409, 2013. https://doi.org/10.3813/AAA.918619

[7] L. Onrubia-Fontangordo, J. M. Bravo Plana-Sala, S. Castiñeira-Ibáñez, and J. V. Sánchez-Pérez, "Design and validation of a comprehensive model to characterize sonic crystals acoustic screens in the low frequency regime," Appl. Acoust., vol. 224, p. 110102, 2024. https://doi.org/10.1016/j.apacoust.2024.110102

[8] J. Redondo, D. Ramírez-Solana, and R. Picó, "Increasing the insertion loss of sonic crystal noise barriers with Helmholtz resonators," Appl. Sci., vol. 13, no. 6, p. 3662, 2023. https://doi.org/10.3390/app13063662

[9] X. Qin, A. Ni, Z. Chen, M. Fang, and Y. Li, "Numerical modeling and field test of sonic crystal acoustic barriers," Environ. Sci. Pollut. Res., vol. 30, no. 6, pp. 16289–16304, 2023. https://doi.org/10.1007/s11356-022-23109-2

[10] D. Ramírez-Solana, J. Galiana-Nieves, R. Picó, J. Redondo, and V. Sangiorgio, "Sonic crystal noise barrier with resonant cavities for train brake noise mitigation," Appl. Sci., vol. 14, no. 7, p. 2753, 2024. https://doi.org/10.3390/app14072753

[11] I. Kralov, K. Nedelchev, E. Gieva, and I. N. Ruskova, "Investigation of the influence of the number of rows in sonic crystal acoustic barriers with cylindrical elements on their acoustic characteristics," AIP Conf. Proc., vol. 2333, p. 060009, 2021. https://doi.org/10.1063/5.0042035

[12] M. Ibarias, V. Cutanda Henríquez, F. Lucklum, and J. Sánchez-Dehesa, "Broadband acoustic absorption at low frequencies by slabs and clusters made of hard cylindrical rods," J. Appl. Phys., vol. 136, p. 044901, 2024. https://doi.org/10.1063/5.0208386

[13] M. Molerón, M. Serra-Garcia, and C. Daraio, "Visco-thermal effects in acoustic metamaterials: from total transmission to total reflection and high absorption," New J. Phys., vol. 18, no. 3, p. 033003, 2016. https://doi.org/10.1088/1367-2630/18/3/033003

[14] X.-H. Zhang and Z. Qu, "Viscous and thermal dissipation during the sound propagation in the continuously graded phononic crystals," Appl. Acoust., vol. 176, p. 108606, 2021. https://doi.org/10.1016/j.apacoust.2021.108606

[15] "COMSOL Multiphysics® software – understand, predict, and optimize," COMSOL Inc. [Online]. Available: https://www.comsol.com/comsol-multiphysics

[16] "Perfectly matched layers (PMLs)," COMSOL Documentation, Pressure Acoustics Module User's Guide. [Online]. Available: https://doc.comsol.com/5.5/doc/com.comsol.help.aco/aco_ug_pressure.05.106.html

[17] International Electrotechnical Commission, IEC 61672-1: 2013 – Electroacoustics: Sound Level Meters, Part 1: Specifications. Geneva, Switzerland: IEC, 2013. [Online]. Available: https://reference.globalspec.com/standard/3890183/iec-61672-1-2013

[18] G. S. Sharma, "Acoustic performance of periodic composite materials," presented at Acoustics 2015 Hunter Valley, Australian Acoustical Society, Hunter Valley, Australia, Nov. 15–18, 2015. [Online]. Available: https://www.acoustics.asn.au/conference_proceedings/AAS2015/papers/p75.pdf

[19] R. G. Sargent, "Verification and validation of simulation models," in Proc. 2011 Winter Simulation Conf. (WSC), Phoenix, AZ, 2011, pp. 183–198. https://doi.org/10.1109/WSC.2011.6147750

[20] D. Handayani, E. F. Ferdyan, S. As'ad, I. Yahya, and Ubaidillah, "Sound barrier model with sonic crystal structure for attenuating noise due to road transportation activity," Evergreen, vol. 11, no. 3, 2024. https://doi.org/10.5109/7236858

[21] F. Brinkmann, L. Aspöck, D. Ackermann, S. Lepa, M. Vorländer, and S. Weinzierl, "A round robin on room acoustical simulation and auralization," J. Acoust. Soc. Am., vol. 145, no. 4, p. 2746, 2019. https://doi.org/10.1121/1.5096178

[22] X. Qin, W. Yang, Z. Zhang, and Z. Chen, "Research on the design and noise reduction performance of periodic noise barriers based on nested structure," J. Clean. Prod., vol. 466, p. 143708, 2024. https://doi.org/10.1016/j.jclepro.2024.143708

[23] J. Galiana Nieves, R. Picó, R. del Rey, J. Alba, and J. Redondo, "Assessment of the sound reduction index provided by noise barriers with low sound insulation," Appl. Acoust., vol. 221, p. 109967, 2024. https://doi.org/10.1016/j.apacoust.2024.109967

[24] Mohapatra, K., & Jena, D. P. (2023). Numerical and experimental methods to measure the acoustic performance of sonic crystal noise barrier. Building Acoustics, 30(3), 339-356. https://doi.org/10.1177/1351010X231179003

Biography

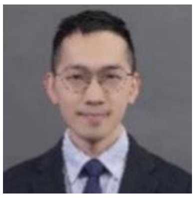

King-cheong Lam is a Senior Lecturer in the Division of Science, Engineering and Health Studies, School of Professional Education and Executive Development, The Hong Kong Polytechnic University. He is actively involved in teaching, curriculum development, and applied research in engineering and technology-related disciplines. His academic and professional work focuses on promoting interdisciplinary education and industry-oriented learning. He has participated in research projects related to engineering applications, computational modelling, and technology-enhanced education. In addition to teaching and research, he contributes to academic programme development and student supervision. His current work emphasises engineering education and practical applications of emerging technologies in industry.

Research Field

King-cheong Lam: Gas sensing, Graphene, DFT calculations, Materials science, Battery
Chin-to Wat: DFT calculations, Materials science, Battery, Applied physics, Engineering education
Syed Bilal Ahmed: DFT calculations, Molecular Motors, Materials science, Applied physics, Engineering education

Chak-yin Tang: Operations research, Systems engineering, Industrial optimization, Logistics and supply chain analytics, Manufacturing systems and automation

Hai-hui Ruan: Solid mechanics and materials, Thermal–fluid sciences, Mechanical design and dynamics, Computational mechanics, Energy systems and heat transfer

Chi-ho Wong: Applied physics, Engineering education, Materials and energy studies, DFT calculations, Superconductor

Kia Ho-yin Tsang: Learning analytics, Machine learning models, Artificial neural networks, Pattern recognition, Intelligent systems

Ricky Kai-long Mak: Business analytics, Operations management, Decision sciences, Systems modelling, Quantitative methods in management

Wai-keung Anthony Loh: Applied physics and engineering, Materials and energy systems, Engineering education, Environmental and health-related applied sciences